Wave Propagation Modeling Capabilities at LLNL: Applications to Regional Discrimination

C. A. Schultz, S.C. Larsen, P. Goldstein, S.D. Ruppert

Earth Sciences Division, Lawrence Livermore National Laboratory
University of California

Sponsored by DOE CTBTR&D Program[1]

ABSTRACT

The numerical synthesis of regional seismograms has become an integral part of Lawrence Livermore National Laboratory's (LLNL) seismic discrimination program. In this paper, we summarize our fundamental approaches to numerical modeling. Our capabilities currently include reflectivity, normal mode, boundary integral, and finite-difference modeling, along with hybrid approaches which utilize two or more of these techniques together. We apply these capabilities to the discriminant variability along three different arrays deployed during the Non-Proliferation Experiment (NPE). Phase amplitudes have been calculated for the approximately three hundred regional stations which recorded the NPE. The majority of these recordings were to the west of the NPE, along one profile of the Southern Sierra Continental Dynamics (SSCD) refraction profile. Based on the three profiles which made up the SSCD refraction experiment, traveltime tomography was utilized to develop a well constrained 3D velocity model across a profile which extends from the Basin and Range, through the southern Sierra Nevada range, the Great Valley, to the San Andreas fault zone in the coastal ranges. The western array of the NPE regional deployment consisted of 285 stations coincident with this SSCD profile. This resulted in phase and discriminant coverage along one of the most well constrained velocity profiles in the western United states. Our analysis shows that although there is amplification of *Pg* and *Lg*, *Pn* has some of the most dramatic variations in amplitude. In California, these amplifications coincide with the western flank of the Sierra Nevada, the eastern quarter of the Great Valley, and the coastal ranges. In Nevada, a dramatic amplification occurred in the Broken Hills volcanic region. To the east, along the Arizona-Utah border, amplification occurred along the transition between the Basin and Range and the Colorado Plateau. The amplification of *Pn* in these regions resulted in a considerable deviation in 6-8 Hz *Pn/Lg* ratios. However, we find that the *Pn/Lg* slope was considerably more stable, showing less variation as a function of distance from the NPE. Numerical modeling with the reflectivity shows that when material contrasts are large enough, a local plane layered structure can result in significant *Pn* amplification. Boundary integral modeling shows that site resonances due to local 2D structure and topography can account for the dramatic amplification and time duration of *Pn* observed in Broken Hills. Finite-difference modeling shows that crustal thickening along the Colorado Plateau can result in focusing which may explain much of the amplification in the 0.5 to 10 Hz frequency band which appears at distances of 200 and 280 km.

[1]Research performed under the auspices of the U.S. Department of Energy by the Lawrence Livermore National Laboratory under contract W-7405-ENG-48.

OBJECTIVES

A primary goal of our research at LLNL has been to develop an assemblage of the most promising numerical techniques for simulating regional wave propagation through complex media. These numerical capabilities will be an integral part of our approach to regional characterization in both the Middle East and North Africa. In this paper, we focus on demonstrating and validating our current modeling capabilities, which include reflectivity, boundary integral, finite-difference, along with hybrid forms of these approaches. We use the boundary integral and finite-difference techniques to provide better understanding of regional discriminant variability along three arrays which were deployed to record regional signals from the NPE. These arrays extend west, northwest, and east from NTS, with the western line coinciding with one of three Southern Sierra Continental Dynamics (SSCD) refraction experiment profiles (Ruppert et al., in press; Fliedner et al., in press). This gives detailed coverage of regional phases along one of the most well constrained crustal profiles in the western United States. Phase amplitudes and the resulting discriminant variability are presented. This "ground truth" dataset will then act as the basis for the future validation of our numerical codes concurrent with our regionalization of the Middle East and North Africa.

RESEARCH ACCOMPLISHED

Current Capabilities

Synthetic modeling of seismic wave propagation in elastic media is an integral part of LLNL's seismic discrimination program. The purpose of our research is to apply a collection of validated wave propagation codes to the Middle East and Northern Africa for discriminant phase analysis. This includes discriminant development, the interpretation of discriminant results, and regional characterization. Our current numerical capabilities for seismic wave propagation include a generalized 1D reflectivity algorithm (Randall, 1994) and a 2D boundary integral algorithm, which generalizes the reflectivity approach to irregular boundaries (Schultz and Toksöz, 1994; Bouchon et al. 1989). Our current finite-difference capabilities consist of a highly optimized 2D/3D wave propagation code, ELAS3D (Levander, 1988; Larsen and Harris, 1993; Larsen, 1995) for modeling full elastic wave propagation in a complex media.

In general, the boundary integral techniques form a very accurate approach to modeling the propagation of P and S waves in an irregularly layered media, allowing for the simple inclusion of free surface topography, irregular boundaries separating homogeneous layers, and attenuation. Unfortunately, the boundary integral techniques are somewhat limited with respect to regional propagation, since the algorithm quickly becomes computationally intensive as the boundary conditions along each interface must be solved with a full general matrix at each independent frequency. Bouchon et al. (in press) have recently shown that the biconjugate gradient approach combined with a threshold cutoff in the matrix can greatly accelerate these algorithms. However, these approaches are still prohibitively large for modeling high frequency responses ($f > 1$ Hz) at regional distances. We, therefore, implement the boundary integral approach more as a site tool for modeling the response of local structure to incident seismic energy. In addition, this code has proven extremely useful for benchmarking the validity of recently developed wave propagation techniques for complex media.

Using the boundary integral technique as a benchmarking tool, we have placed a major emphasis on making finite-difference an accurate and viable tool for modeling wave propagation at regional distances. ELAS3D has become a highly optimized 2D/3D finite-difference algorithm which is fourth-order accurate in space and second order accurate in time. This code has a run-time visualization feature and post-processing capabilities. A variable density grid has been implemented, yielding significant savings in computer speed and memory. We have incorporated both active grid and a propagating envelope algorithms. These speed up the code by eliminating calculations in regions which are void of "interesting" seismic energy. In addition, we have implemented a very efficient scheme for modeling

the response of free surface topography in the 2D portion of the code. This implementation is currently undergoing rigorous testing.

We have ported ELAS3D to several platforms including the Sun workstations, SGI, IBM 2000, and the Cray Y-MP, giving us the ability to model wave propagation at regional distances. Since numerical dispersion resulting from coarse grid sampling is the greatest limitation to propagation at larger distances, we have started implementing ELAS3D on a massively parallel processor to increase the spatial sampling rate. We have since ported a simpler acoustic version of the code to LLNL's 256-processor Meiko CS-2 where we observed a speed of 28 GFLOPS. Initial tests show that the parallelized version of the full elastic code will dramatically decrease the current run-time while significantly increasing the available memory. The largest predicted 2D model is 300 x 3000 kilometers at 10 Hz, given a constant P-wave velocity of 5 km/s. The time to compute a full seismogram on this grid is on the order of a week. Considering a typical regional propagation distance to be on the order of 50 x 500 km, there is ample memory to increase the sampling rate above the minimum limit of ten points per wavelength, thereby reducing numerical dispersion considerably. In the 3D case, the largest possible model is 25 x 25 x 25 kilometers at 10 Hz given the constant P-wave velocity of 5 km/s. The time to compute a whole seismogram is on the order of only a few hours.

Application to Discriminant variability

An improved understanding of the variability of regional seismic phases with distance is needed to improve the performance and transportability of regional seismic discriminants. Numerous studies, in a number of regions, have observed large variations in each of the dominant regional phases. Studies have shown large variations in *Pn*, *Sn*, and *Lg* over relatively short distances (e.g. Keller et al., 1994; Kadinsky-Cade et al., 1981; Ni and Barazangi, 1983). An improved understanding of these variations has been gained from numerous empirical studies (e.g. Chavez and Priestley, 1986; Zhang et al., 1994) and theoretical studies (e.g. Campillo, 1990; Kennett, 1993). The numerical approaches discussed in the section above, give us the tools to compliment these previous studies and gain physical insight into the propagation of phases, thereby allowing us to better understand the transportability of discriminants.

As part of our efforts to develop procedures for regional geophysical characterization, we have been making and assembling empirical observations of regional phase propagation. At the same time, we have been interpreting these observations with our numerical modeling to describe the observed phenomena. Examples include measurements and modeling of the variability of regional *Pn*, *Pg*, and *Lg* signals from the NPE along lines to the east, west, and northwest. Figure 1 shows the three arrays deployed to record regional phases propagating from the NPE. The 330 km long Nevada array extends from the NPE northward through the Basin and Range province of northwestern Nevada. The 300 km Arizona array extends eastward from the Basin and Range crossing over to the Colorado plateau, while the Sierra array is a 460 km profile which extends across one of the most rugged profiles in the western United States. This profile crosses Owen's Valley, the Sierra Nevada Ranges, the Great Valley, and finally terminates just short of the San Andreas fault zone. The average station separation along the Sierra line is less than 2 kilometers, giving excellent station coverage of regional phases.

Observations and modeling of variations in regional phases, both with distance and from region to region, are important because the detection, location, and identification of small magnitude events rely heavily on observation of these phases. For example, one of the most popular regional discriminants is based on the ratio of high-frequency (e.g. 6-8 Hz) *Pn* to *Lg* spectral amplitudes. If one of these phases is more sensitive to variations in structure such as Moho depth or topography, we would expect to observe significant variations from station to station, or at a single station for events from different azimuths. Figure 2 shows recordings of the NPE along the line that extends across the Sierra Nevada Range and Figure 3a demonstrates the variability in the discriminants. We find that large variations in *Pn* map

directly into the 6-8 Hz *Pn/Lg* spectral amplitude ratio. Variations do exist in *Lg*, although they tend to be much smaller than those in *Pn*. If such variations are due to systematic changes in features like crustal thickness or topography, they would be very sensitive to source-receiver distance or azimuth, potentially introducing large variability into discriminants such as *Pn/Lg* spectral ratios. Based on the SSCD refraction experiment (Ruppert et al., in press; Fliedner et al., in press), travel time tomography has been used to attain a 3D "ground truth" velocity model for both the crust and mantle in this region using data from 24 shots and three profiles. We are utilizing this profile for code validation as we try to better define our ability to predict observed variations in regional phases. This testing will continue and improvements will be made concurrent with our efforts of regional characterization in the Middle East and North Africa.

The 6-8 Hz spectral amplitude of the three most dominant regional phases is plotted as a function of position on Figure 1. There is a substantial amount of variation in the amplitude of the regional phases, the most dramatic variations being in the *Pn* phase while both the *Pg* and *Lg* phases have less variation with distance. Although variability of these three regional phases are minimal as they pass through northwestern Nevada, there is an order of magnitude amplification at the Broken Hills site near Fallon, Nevada. *Pn* is amplified by almost an order of magnitude relative to the surrounding stations, while *Pg* and *Lg* are amplified by only a factor of two. Figure 4 shows two proposed structures based on the little that we know of the geology at this site (Vitaliano, 1957) and the observation that much of the amplification consists of a 6 Hz resonance. Modeling with reflectivity shows that although the spectral shape and the drawn out time domain signal can be generated with two low velocity volcanic layers, one at the surface and the other a few hundred meters deep, at most only a four time amplification factor is predicted. Boundary integral modeling of a basin consisting of hydrothermally altered low-velocity volcanics with local topography demonstrates that 2D site structure can extend the time duration of the *Pn* signal and provide the additional amplification observed at the site.

The Arizona line also shows a large variation in *Pn* with distance, while *Lg* again tends to be more stable in spectral amplitude at 6-8 Hz. However, the oblique polarization of *Pn* at the site of amplification strongly suggests that the source of this amplification is a deeper focusing mechanism. Zandt (1995) has shown that raytracing combined with geologic and geophysical control along this profile predict crustal thickening along the transition between the Basin and Range and the Colorado Plateau, resulting in two consecutive Moho steps and significant lateral velocity variations. This model predicts focusing at the stations where *Pn* appears amplified in Figure 1. Finite-difference synthetics, shown in Figure 5, predict a similar amplification of *Pn* at the corresponding regional distances. Utilizing the broadband nature of this finite-difference modeling, this step is over a large enough distance that, in addition to the observed amplification at 6 Hz, significant amplification occurs over the full 0.5 to 10 Hz range typically utilized in regional discriminant analysis.

CONCLUSIONS AND RECOMMENDATIONS

LLNL will continue to develop a numerical foundation for the synthesis of seismograms at regional distances. We have developed a "ground truth" database across the southern Sierra Nevadas which will be used for the continued validation of our numerical modeling capabilities. In addition, future enhancements will be made to ELAS3D which include 3D implementations of attenuation, topography, and variable density grids, along with a 2.5D axial-symmetric option. This code will be made available on a number of additional platforms including workstation clusters.

Integrating these numerical algorithms with our empirical study of phase and discriminant variability in the southwestern United States, we have demonstrated the great variability of *Pn* due to crustal thickening and local site resonances, especially as observed in regions containing low-velocity layers. Examples include the crustal thickening of the Colorado Plateau and Sierra Nevada range and near surface low velocity structure in the Great Valley and Broken Hills region. The low velocity resonances

tend to amplify *Pn* both due to the resonance itself and the vertical polarization of *Pn*. Even though *Lg* is amplified by these low velocities it becomes radially polarized, significantly reducing the amplitude on the vertical component. Therefore, the vertical component shows an anomalously large *Pn/Lg* ratio, potentially introducing the risk of false alarms. This emphasizes the importance of three-component analysis when transporting these discriminants to different regions. One example where numerical calculations can lead to insights about discriminant performance is the *Pn/Lg* slope discriminant (Goldstein, 1995). This discriminant may be more stable than taking a *Pn/Lg* ratio in a narrow frequency band because of the inherent averaging that occurs over narrow band resonances.

Acknowledgments. Research was performed under the auspices of the U.S. Department of Energy by the Lawrence Livermore National Laboratory under contract W-7405-ENG-48.

References

Bouchon, M., M. Campillo, & S. Gaffet, 1989, A boundary integral equation-discrete wavenumber representation method to study wave propagation in multilayered media having irregular interfaces, *Geophysics*, **54**, 1134-1140.

Bouchon, M., C. A. Schultz, & M. N. Toksöz, 1995, A fast implementation of boundary integral equation methods to calculate the propagation of seismic waves in laterally-varying media, *Bull. Seism. Soc. Am.*, submitted.

Campillo, M., 1990, Propagation and attenuation characteristics of the crustal phase *Lg*, *Pure Appl. Geophys.*, **13**, 1-19.

Chavez, D. A. & K.F. Priestley, 1986, Measurement of frequency dependent *Lg* attenuation in the Great Basin, *Geophys. Res. Lett.*, **13**, 551-554.

Fliedner, M. & S. D. Ruppert, Three-dimensional crustal structure of the southern Sierra from seismic fan profiles and gravity modeling, *Geol.*, in press.

Goldstein, P., 1995, Slopes of P- to S-wave spectral ratios: a broadband regional seismic discriminant and a physical model, UCRL-JC-121223.

Kadinsky-Cade, K., M. Barazangi, J. Oliver, & B. Isacks, 1981, Lateral variations of high-frequency seismic wave propagation at regional distances across the Turkish and Iranian plateaus, *J. Geophys. Res.*, **86**, 9377-9369.

Keller, G. R., P. E. Malin, & S. D. Ruppert, 1994, Southern Sierra Nevada Continental Dynamics Project: 1993 field observations of the NPE, *DOE symposium on the Non-Proliferation Experiment, April 19-21*, Rockville Maryland.

Kennett, B. L., 1993, The distance dependence of regional phase discriminants, *Bull. Seism. Soc. Am.*, **83**, 1155-1166.

Larsen, S.C., 1995, 3D MPP simulations in the earth sciences: seismic applications, LLNL Symposium on Distributed Computing and Massively Parallel Processing.

Larsen, S.C. & D.B. Harris, 1993, Seismic wave propagation through a low velocity nuclear rubble zone, UCRL-ID-115729.

Levander, A., R., 1988, Fourth-order finite-difference P-SV seismograms, *Geophys.*, **53**, 1425-1436.

Ni, J. & Barazangi, High-frequency seismic wave propagation beneath the Indian Shield, Himalayan Arc, Tibetan Plateau and surrounding regions: high uppermost mantle velocities and efficient Sn propagation beneath Tibet, *Geophys. J. Roy. Astr. Soc.*, **72**, 665-689.

Randall, G.E., 1994, Efficient calculation of complete differential seismograms for lateral homogeneous earth models, *Geophys. J. Int.*, **118**, 245-254.

Ruppert, S. D. & Fliedner, M., Crustal structure and thickness of the southern Sierra Nevada from seismic refraction profiles, *Geol.*, submitted.

Schultz, C. A. & M. N. Toksöz, 1994, Enhanced backscattering of seismic waves from a highly irregular, random interface: P-SV case, *Geophys. J. Int.*, **117**, 783-810.

Vitaliano, C.J., 1957, Wall-rock alteration in the Broken Hills Range, Nevada, *J. Geol.*, **65**, 167-77.

Zandt, G., 1995, Crust and mantle structure across the Basin and Range-Colorado Plateau boundary at 37N latitude and implications for Cenozoic extensional mechanism, *J. Geophys. Res.*, **100**, 10529-548.

Zhang, T.R., S.Y. Schwartz, & T. Lay, Multivariate analysis of waveguide effects on short-period regional wave propagation in Eurasia and its application in seismic discrimination, *J. Geophys. Res.*, **99**, 21929-945.

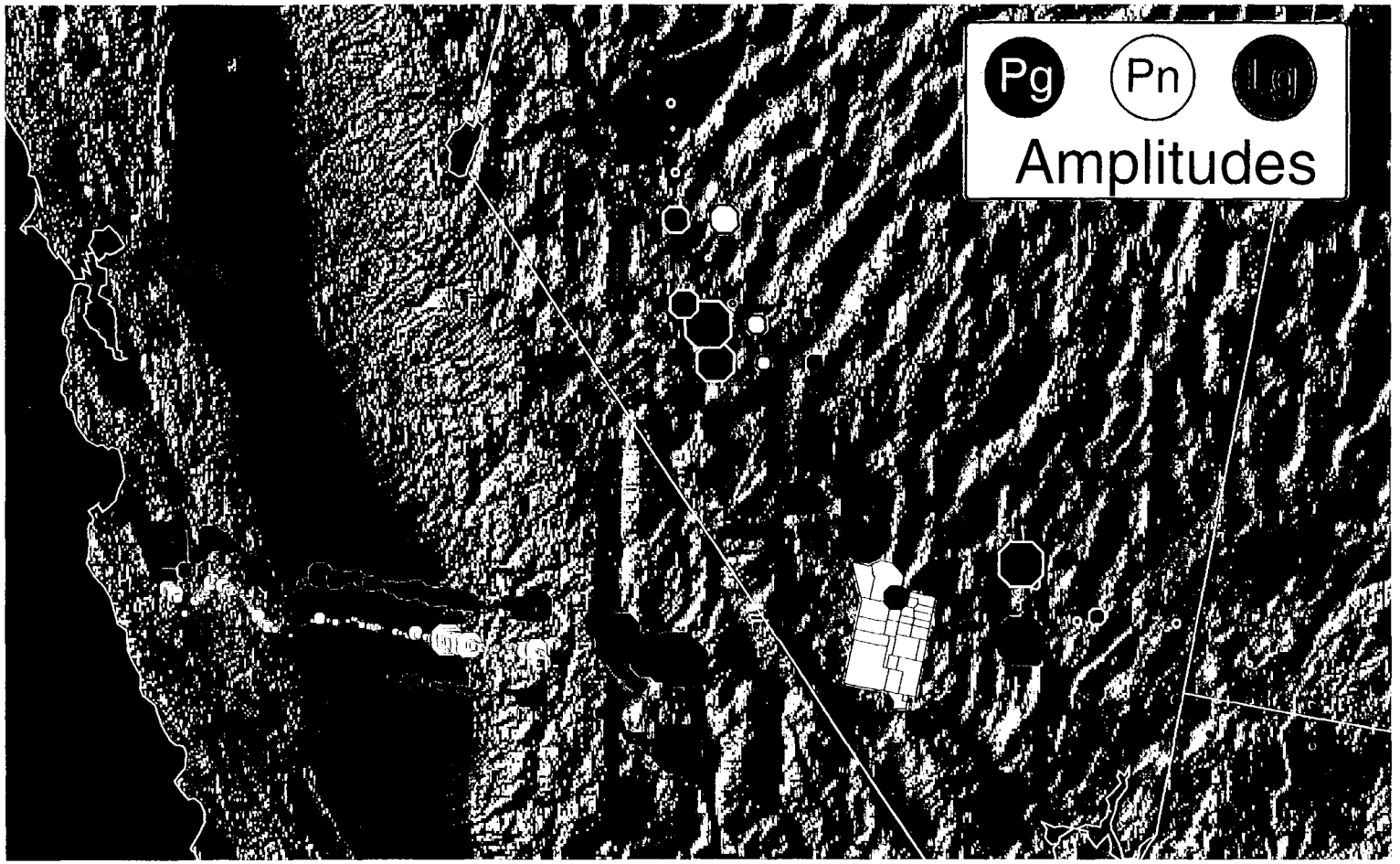

Figure 1: Spectral amplitude in the 6-8 Hz range for *Pn*, *Pg*, and *Lg* phases along each of the three arrays deployed during the NPE. The three phase amplitudes are plotted side by side along each array so that *Pn* is plotted over the actual station location and *Pg* and *Lg* are plotted to each side of the station location. Data is normalized for each independent array to the single largest phase amplitude recorded at a station along the array. A distance correction has not been applied to this data.

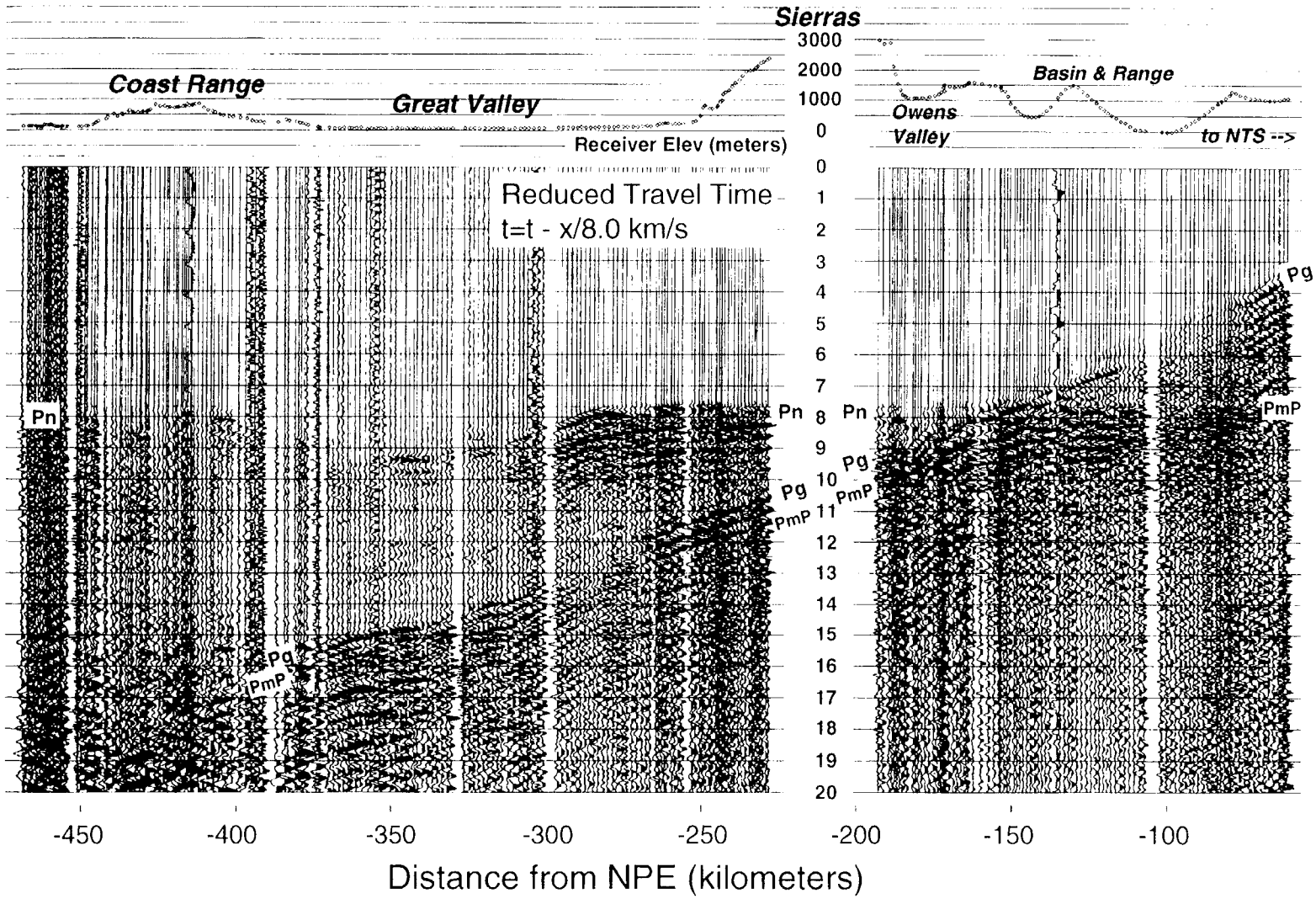

Figure 2: Plot of the regional seismograms recorded along the western array. Data is trace normalized to emphasize phases at the larger offsets. *Lg* arrives outside the time window shown.

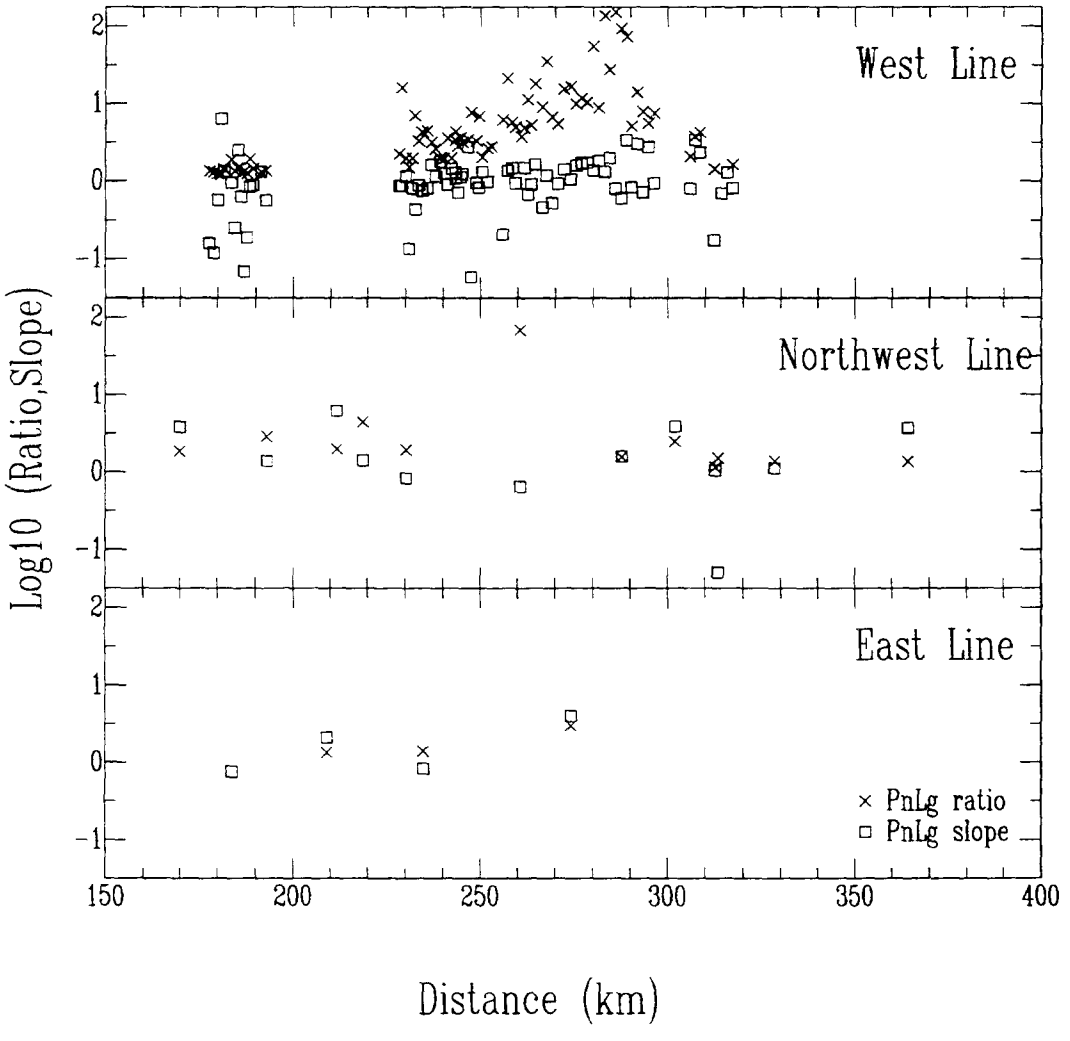

Figure 3: Two commonly used discriminants, the *Pn/Lg* ratio in the 6-8 Hz band and *Pn/Lg* slope over the full spectral range, calculated along the three seismic lines deployed for the NPE. We have applied a preliminary distance correction to this data. The lower outliers in the *Pn/Lg* slope are partially due to a low signal-to-noise criterion.

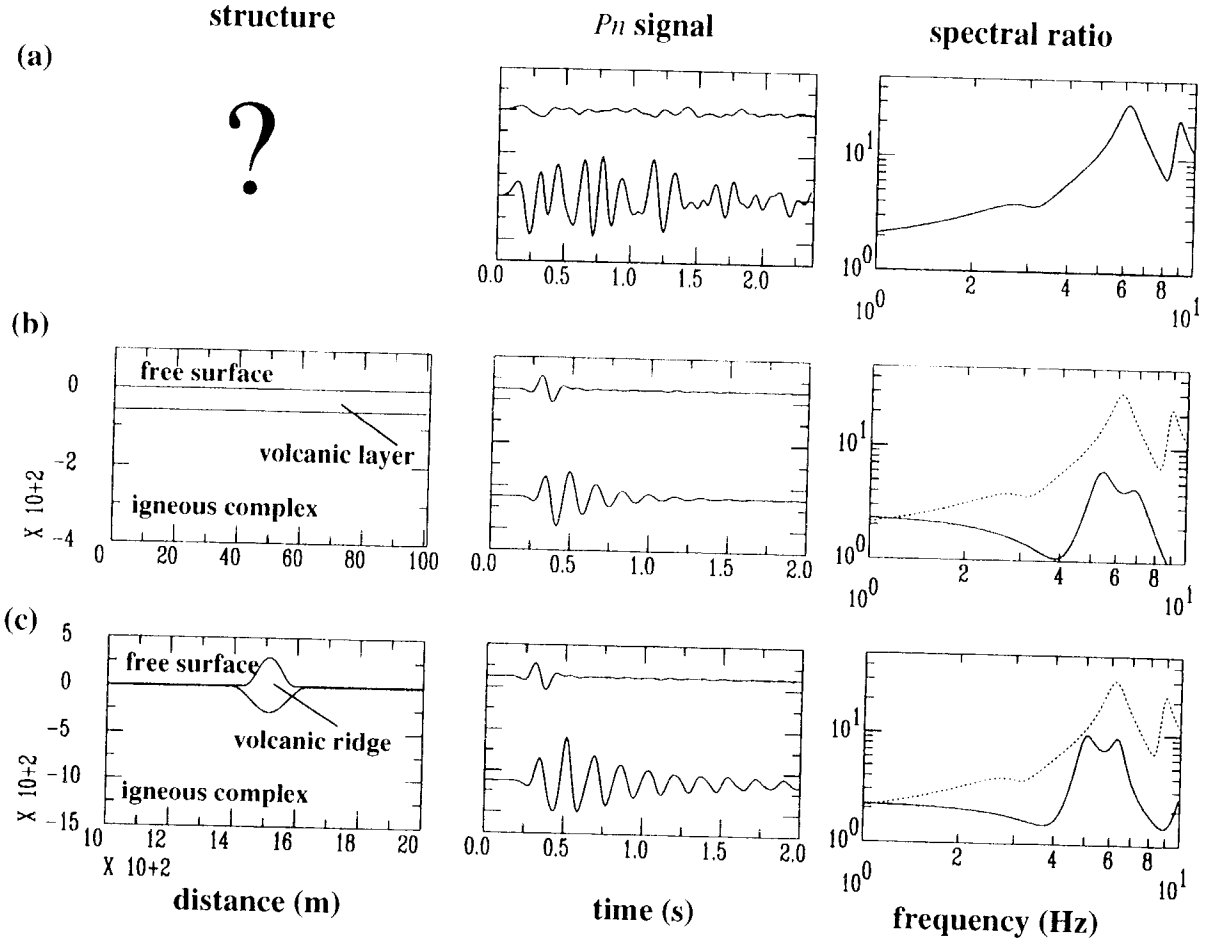

Figure 4: Comparison of (a) the anomalous *Pn* phase observed along the northwest line with an adjacent station approximately 20 km away. The dramatic 6 Hz amplification can be seen at this site. This *Pn* amplification is modeled with an igneous body covered by (b) a low velocity volcanic layer and (c) a low velocity volcanic ridge. A reference case corresponding to the response of a homogeneous igneous body is also given on the same plot. In all cases, the spectral ratios are given to show the general site amplification. The observed spectral ratio is shown for reference in the synthetic results.

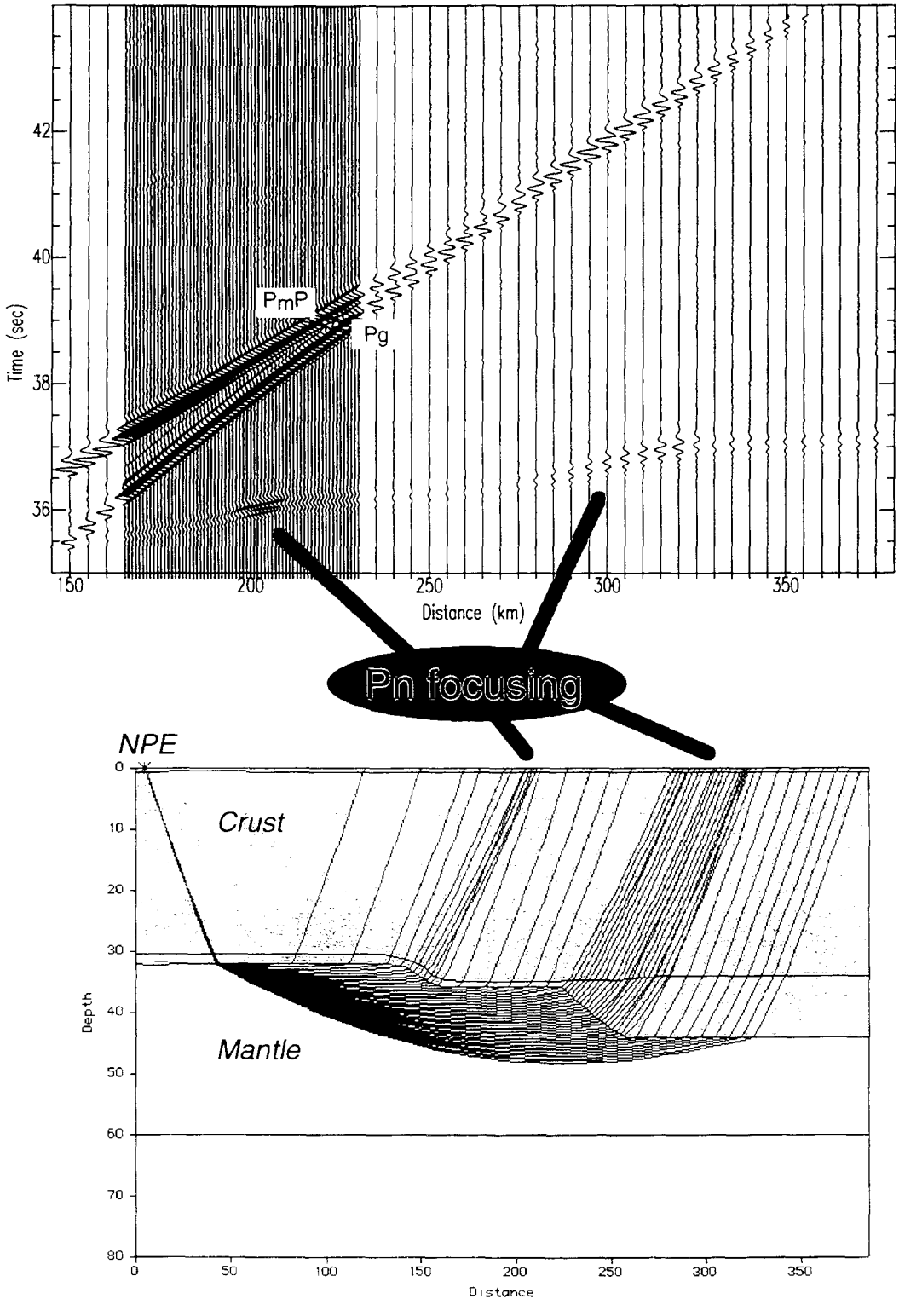

Figure 5: Finite-difference synthetics showing the response of the *Pn* and *Pg* phases to crustal thickening along the transition between the Basin and Range and the Colorado Plateau. At 200 km the *Pn* is amplified by approximately a factor of three due to focusing from a Moho step.